Giant Grüneisen parameter in a superconducting quantum paraelectric

J. Franklin[1], B. Xu[1], D. Davino[1], Aditi Mahabir[1], A. V. Balatsky[1,2], U. Aschauer[3], I. Sochnikov[1,4]

[1]*Physics Department, University of Connecticut, Storrs, CT USA, 06269*
[2] *Nordita, KTH Royal Institute of Technology and Stockholm University, Roslagstullsbacken 23, SE-106 91 Stockholm, Sweden*
[3]*Department of Chemistry and Biochemistry, University of Bern, Bern Switzerland*
[4]*Institue of Material Science, University of Connecticut, Storrs, CT USA, 06269*

Superconductivity and ferroelectricity are typically thought of as incompatible because the former needs free carriers, but the latter is usually suppressed by free carriers. This is unless the carrier concentration is sufficiently low to allow for polar distortions and mobile electrons to cooperate. In the case of strontium titanate with low carrier concentration, superconductivity and ferroelectricity have been shown to be correlated via various tuning methods, such as strain. Here, we report theoretically and experimentally evaluated Grüneisen parameters whose divergent giant values under tensile stress indicate that the dominant phonon mode which enhances the superconducting order is the ferroelectric transverse soft phonon mode. This finding puts strong constraints on other phonon modes as the main contributors to the enhanced superconductivity in strained strontium titanate. The methodology shown here can be applied to strain-tune and probe properties of other materials with polar distortions including topologically non-trivial ones.

Superconducting polar metals have attracted recent interest due to both their potential for creating new unconventional superconductors and for their potential for applications such as superconducting memory controlled by ferroelectric polarization. Materials with proven or possible connections of a polar nature and superconductivity include, but are not limited to WTe_2 [1,2], $KTaO_3$ [3], PbTe [4], BiTeI [5,6] and doped $SrTiO_3$ [7]. Some of these materials are supposed to be topologically non-trivial [1,2]. While the detailed physics varies among these materials, a common feature is the presence of polarization at low electron doping. While these materials offer a fascinating toolbox for multi-order correlations and topology, exactly how the superconducting states are formed and what the unconventional aspects of those states are present open fundamental questions [8]. Put simply, we know these materials superconduct, we know that some have substantial spin-orbit coupling and non-trivial bands, but we do not know why and what type of unconventional superconducting pairing exist in these materials [7]. The methodology presented below can be applied to advance our understanding of many of these materials.

Here we focus on strontium titanate ($SrTiO_3$) which has one of the lowest carrier densities among low-carrier-density superconductors (the only real 'competitor' being twisted bilayer graphene [9]). It has been known for many decades that the Fermi energy in $SrTiO_3$ is low compared to the naïvely estimated Debye energy, which makes application of BCS theory impossible, see references in a recent review article [7]. Despite the increased research activity in recent years [7], the nature of the low-carrier-concentration superconducting state in $SrTiO_3$ is still an unresolved fundamental mystery and is a major challenge to the field of quantum materials and unconventional superconductors.

The recent debate about appropriate models [10–21,7] mostly swirls around the question of which phonons provide the superconducting pairing and how. Showing experimentally which phonons are the most relevant is not a trivial task either: Some recent experiments on approaching the quantum paraelectric to ferroelectric phase transition show correlations of the ferroelectric phase with superconductivity [22–28]. However, most of these observations are rather qualitative, and have mainly shown the mere correlations of the tuning parameter with the change in critical temperatures. The current work provides a more clear *quantitative* link between macroscopic observations and the microscopic parameters of the interacting ferroelectric and superconducting phases in this enigmatic material.

The two most striking findings we report here are: (a) the Grüneisen parameter in $SrTiO_3$ reaches gigantic values on the order of several thousands, larger than previously reported in many conventional and unconventional materials [29–35], and (b) these values agree with our theoretical calculations within the inspected strain ranges. These findings provide a clear,

consistent evidence that the response of the superconducting phase to strain is predominantly due to the soft, so-called transverse optic (TO), ferroelectric phonon mode with displacements along the tensile strained *c*-axis direction. The importance of these findings is to show that no other phonons, including the longitudinal ferroelectric branches, contribute noticeably to the anomaly in the response.

In the following sections, we first provide a broad introduction to the Grüneisen parameter. Then we present the theory portion of the manuscript in two parts. The first part is an analytical argument that outlines a link between the superconducting critical temperature and the soft-mode frequency. This part also includes the ansatz that the strain in the sample is non-uniform, resulting in a distribution of critical temperatures. The second theory part presents DFT calculations of the phonon spectrum that show that only one phonon has a significant strain dependence. We then compare these insights with the experimental data and close the paper with an argument that when combined, these findings show that the transverse optical ferroelectric mode plays a crucial role in the superconducting pairing.

The thermal expansion of superconductors and other materials [36–40] can be efficiently described using the *thermodynamic* Grüneisen parameter, which, at finite temperatures, is determined by the volume dependence of the entropy through its logarithmic derivative [41]. The thermal expansion comes from the pressure of electrons due to the occupancy change of the Fermi surface and the population of higher energy vibrational phonons states, *i.e.* frequency dependence on strain [38,42]. Therefore, in general, both electronic and phononic contributions to the thermal expansion or to the *microscopic* Grüneisen parameters should be expected in a conducting material (ignoring magnetic orders for the purpose of this discussion). The Grüneisen functions for the normal and superconducting states mainly differ in their electronic components. Furthermore, the Grüneisen parameters depend on the volume dependence of the electron-phonon interaction. At temperatures close to zero, which is the relevant range for materials near quantum critical points, entropy derivatives can be directly related to the free energy pertaining to the quantum critical point [43]. Following these strategies, we define the *thermodynamic superconducting* Grüneisen parameter:

$$\gamma_s(V) = \frac{d\ln(F_n - F_s)}{d\ln V}, \tag{1}$$

where $F_c = F_n - F_s$ is the energy difference between the normal and superconducting states and V is the volume. Within a BCS-like approach, $F_c = N_0\Delta_0^2/2$, where N_0 is the density of states near the Fermi level, and Δ_0 is the superconducting order parameter. With an approximately volume-independent density of states (see Appendix), the superconducting Grüneisen parameter from Eq. (1) depends on the critical temperature, T_c, as

$$\gamma_s(V) \approx \frac{2d\ln T_c}{d\ln V}. \tag{2}$$

The soft-mode superconducting pairing ansatz by Edge et al. [10] states that the critical temperature of strontium titanate depends on the soft-phonon frequency, ω_0, and density of states $\alpha^2F(\omega_0)$, as

$$T_c = \epsilon_F e^{-\frac{\omega_0}{\alpha^2 F(\omega_0)}}, \tag{3}$$

with $\omega_0 = \bar{\omega}|\varepsilon_0 - \varepsilon|^{z\nu}$, where $\bar{\omega}$ is the zero strain transverse ferroelectric phonon mode frequency, ε is the applied strain, ε_0 is the critical strain, and $z\nu$ are scaling critical exponents. Hereafter, we assume an approach from the paraelectric phase. Combining Eq. (2) and (3), with detailed steps shown in the Appendix, under an assumption that $\alpha^2F(\omega_0)$ is approximately independent of ω_0, we obtain that the superconducting Grüneisen parameter and the critical temperature are expected to diverge near the critical strain according to:

$$\begin{aligned} \frac{d\ln T_c}{d\ln \varepsilon} &\approx O(1)\cdot\frac{d\omega_0}{d\varepsilon} \\ &\approx O(1)\cdot(\varepsilon_0-\varepsilon)^{z\nu-1} \end{aligned} \tag{4}$$

This power-law expression, in principle, allows for direct testing of the soft-mode ansatz using experimental data which is also supported by the numerical calculations of phonon frequencies shown in the following paragraphs. However, as we show below, the experimental data does not follow this predicted behavior, but rather a power law $\gamma_s \propto \varepsilon^{\eta}$ form. This is explained assuming inhomogeneous strain (and T_c) as described in detail in the appendix.

Directly related to the thermodynamic Grüneisen parameters, the microscopic mode Grüneisen parameter measures the effect of the population of higher energy vibrational states on the lattice expansion [42]. As already implied by Eq. (4), in our case the mode Grüneisen parameter plays a crucial role related to the superconductivity and the soft ferroelectric mode. Historically, due to large number of hydrostatic pressure experiments compared to uniaxial stress-strain experiments, the *mode* Grüneisen parameter is defined as a volumetric logarithmic derivative of the phonon frequencies $\gamma_{n,\boldsymbol{q}}(V) = \sum_{n,\boldsymbol{q}} \frac{dln(\omega_{n,\boldsymbol{q}})}{dlnV}$, where $\omega_{n,\boldsymbol{q}}$ is the n-th phonon branch at a vector $\boldsymbol{q}$. However, for our experiments, rather than using the volumetric response, we define the mode Grüneisen parameters for the phononic response *to uniaxial strain* as $\gamma_{n,ij,\boldsymbol{q}}(\varepsilon) = -\frac{1}{\omega_{n,\boldsymbol{q}}}\frac{\partial\omega_{n,\boldsymbol{q}}}{\partial\varepsilon_{ij}}$, where $\omega_{n,\boldsymbol{q}}$ is the frequency of a phonon mode n, i and j are the strain tensor indices and $\boldsymbol{q}$ is the phonon wavevector [44]. Furthermore, in experiments under uniaxial *stress* the modes' responses are superimposed, as oftentimes the experimental strain is not in its irreducible form. Thus, a superposition of the *uniaxial strain* mode Grüneisen parameters should be used. In our experiments, a uniaxial stress along the *c*-axis is applied and the strain in the same direction is monitored [1–3]. Assuming weakly coupled phonon modes and a positive Poisson ratio under given strain-stress conditions, we can approximate [46] the effective *c*-axis Grüneisen parameter as a weighted sum $\gamma(\varepsilon_c) = \sum_{n,\boldsymbol{q}}\left(\gamma_{n,\boldsymbol{q}}(\varepsilon_c)\right) \approx \sum_{n,\boldsymbol{q}}\left(-\frac{(1-2\upsilon)}{\omega_{n,\boldsymbol{q}}}\frac{\partial\omega_{n,\boldsymbol{q}}}{\partial\varepsilon_c}\right)$, where $\upsilon \approx 0.28$ is the low temperature Poisson's ratio for $SrTiO_3$ [46], and the sum is over all phonon

modes n and wave vectors $\boldsymbol{q}$. This quantity, $\gamma(\varepsilon_c)$, is derived in our experiments and is shown to be divergent, and will be compared the analogous modelled parameter defined in the following paragraphs.

The above expression assumes isotropy even though strontium titanite is not isotropic. This assumption is satisfactory for emphasizing the main point about the origin of the anomalous response from the ferroelectric soft-mode. For a more complex and rigorous theoretical treatment of anisotropic materials see M. Mito *et al.* [45]. We will make a further simplification in the following discussion by inspecting the Grüneisen parameters at the Γ point only, i. e. $\boldsymbol{q} = 0$. This is motivated by the fact that in our computational supercell the cubic zone-boundary modes are folded back to the Γ point, and by the fact that no anomalous response to strain was detected at intermediate wave-vectors in our calculations.

DFT calculations, the results of which are shown in Figure 1, were performed within the VASP code [50–53] using the PBEsol exchange correlation functional [54] and projector-augmented wave (PAW) potentials [55,56] with Sr(4*s*, 4*p*, 5*s*), Ti(3*p*, 3*d*, 4*s*) and O(2*s*, 2*p*) valence electrons. Wavefunctions were expanded in planewaves up to a kinetic-energy cutoff of 550 eV. We relaxed the lattice parameters and internal coordinates until forces converged below 10^{-5} eV/Å and stress converged below $5{\cdot}10^{-7}$ eV/Å^3. All calculations were performed for 40-atom 2x2x2 supercells of the unit cell that contained the tetragonal distortion corresponding to an $a^0a^0c^-$ rotation of the octahedra in Glazer notation [57]. Reciprocal space was sampled using a 4x4x4 Monkhorst-Pack [58] mesh for this supercell. Phonon frequencies were computed at the Γ-point within the frozen phonon approach, which was implemented in the Phonopy code [58]. We note that results are presented without the non-analytical LO-TO splitting correction, which by definition vanishes in doped STO. Mode Grüneisen parameters were computed as the volumetric derivative under *c*-axis stress $\gamma_n(V_c) = -\frac{V}{\omega_n}\frac{\partial\omega_n}{\partial V_c} = -\frac{1}{(1-2\upsilon)\omega_n}\frac{\partial\omega_n}{\partial\varepsilon_c} \equiv \frac{\gamma_{n,\boldsymbol{q}=0}(\varepsilon_c)}{(1-2\upsilon)}$. The derivative was evaluated by central finite differences, connecting modes at adjacent volumes via the similarity of their eigenvectors. The denominator with the Poisson's ratio, υ, allows the translation of the Grüneisen parameter calculated based on volume $\gamma_n(V_c)$ to the strain-based $\gamma_n(\varepsilon_c)$, to match the tuning deformations used in our experiment. The volume was modulated by applying strain along the *c* axis, and then relaxing the cell shape, volume and all internal coordinates while keeping *c* fixed. In other words, every structural parameter except for the out-of-plane lattice parameter was allowed to relax, in full consistency with the experimental conditions.

Within the investigated range of *c* lattice parameters only the ferroelectric mode along *c* changes from unstable (negative) at large *c* to stable at small *c*, see Figure 1 (upper panel). All other modes show a much smaller dependence on strain along *c*. Notably, the doubly degenerate in-plane ferroelectric mode remains unstable at all *c*. These observed instabilities are in agreement with the quantum paraelectric nature of $SrTiO_3$ that manifests as unstable phonon modes in our 0K DFT calculations without zero-point energy corrections [59,60]. Consequently,

the Grüneisen parameter (Figure 1, lower panel) of the ferroelectric mode along *c* is much larger, by two to three orders of magnitude, than the one for all other modes and shows the divergence expected from its definition at the critical *c* lattice parameter [43]. We want to note that the modes shown in this figure also include zone boundary modes such as octahedral rotations because these modes are folded back to the Γ-point within our supercell. Because of the relevant magnitude of the Grüneisen parameters, these findings rule out any mode other than the ferroelectric transverse phonon modes as main contributors to enhanced superconductivity.

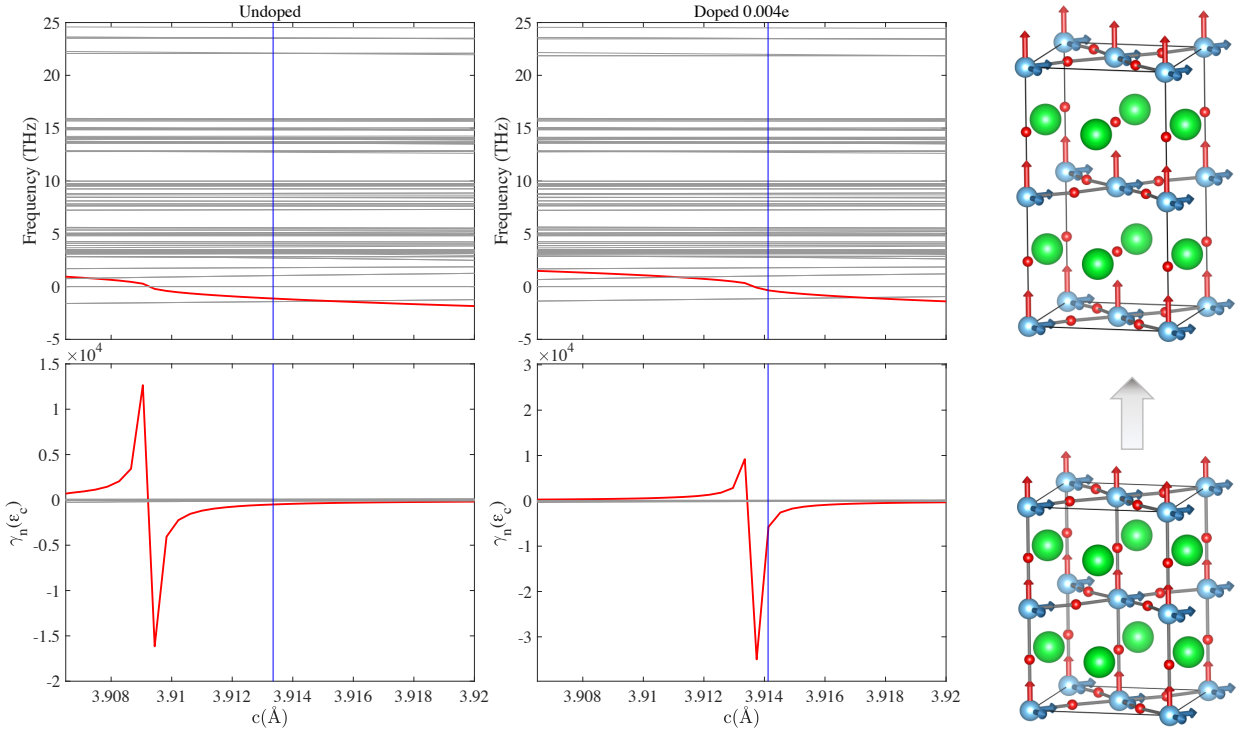

Figure 1. Theoretical phonon frequencies (top plots) and mode Grüneisen parameters, $\gamma_n(\varepsilon_c)$, (bottom plots) calculated as a function of the c lattice parameter for undoped and doped $SrTiO_3$. The calculations are for the antiferrodistortive, not cubic, phase and at 0 K. Vertical lines are equilibrium lattice constants and phonon frequencies are shown without LO-TO splitting. The ferroelectric mode with vibrations along the c-axis is highlighted in red, while all other modes are shown in grey. Only the transverse ferroelectric mode along the c-axis shows large values of the Grüneisen parameter (bottom). Shown to the right is an illustration of the unstrained strontium titanate unit cell (bottom) and the strained one (top). Red, green and blue spheres are oxygen, strontium and titanium ions respectively. The blue and red errors indicate the relative amplitudes of perpendicular and parallel to c-axis branches of the transverse ferroelectric mode, respectively. The branch of the transverse ferroelectric mode with polarization parallel to the c-axis acquires larger

amplitude due to the phonon softening under the tensile deformation indicated by the gray arrow.

Various related types of Grüneisen parameters have been successfully used in the past to unravel details about quantum phase transitions [36,39,43,61]. In $SrTiO_3$, to understand the experimental relationship between strain and the superconducting T_c near the quantum paraelectric phase transition on a quantitative level, we investigate the relevant experimentally measured uniaxial *strain superconducting* Grüneisen parameter defined here in accord with Eqs. (1) and (2), as $\gamma_s(\varepsilon_c) = 2\frac{d\ln T_c}{d\varepsilon_c} = 2\frac{\mathrm{d}T_c}{T_c(\varepsilon_c)\mathrm{d}\varepsilon_c}$, where ε_c is the measured strain along the *c*-axis and T_c is the superconducting transition temperature [43,61,62].

To refocus our derivations on the experimentally revenant notation, we emphasize that we will compare only two Grüneisen parameters, the *macroscopic* $\gamma_s(\varepsilon_c)$ defined for the derivative of the critical temperature and the *microscopic* $\gamma(\varepsilon_c) = \sum_n \gamma_n(\varepsilon_c)$ summed over all phonon modes, which will be dominated by the divergent TO mode. The two Grüneisen parameters are expected to be equivalent with good approximation near the superconducting phase transition under the assumtion that the electronic behavior is dominated by the single energy scale [43] of the superconducting pairing, T_c, and that the electronic and phononic properties are linked through electron-phonon coupling [21,48,49]. This equivalence is what allows for direct conclusions about the microscopic phonon behavior based on the thermodynamic bulk T_c measurements under strain.

The experiments were performed on single crystals of Nb-doped strontium titanate, $SrTi_{0.996}Nb_{0.004}O_3$, in a dilution refrigerator setup with a custom-built strain-stress cell [63] and a polarizing optical microscope [26]. Details of the basic characteristics of the samples are provided elsewhere [26]. Ultra-low excitation currents and an ultra-low noise amplifier and resistance bridge were employed [27,45] to determine the critical temperature, T_c. Stress was applied parallel to the long side of a 0.3 x 2 x 10 mm^3 single crystal sample to define the *c*-axis. The sample's resultant strain along the stress direction was precisely measured using an attached resistive strain gauge. A single doping level is reported here, which is supposedly the closest to the softening of the phonon according to the calculations here and in Ref. [10]. However additional data from another doping level in Ref. [26] shows divergence-like behavior, while much lower and much higher doping samples did not reach high strains due to brittleness.

We measured the resistive signature of the superconducting transition and defined T_c at different normal resistance, R_n, thresholds. Typical critical temperature data are shown in Figure 2 (upper panel)**.** Overall T_c increased by ~30% before the sample fractured. What is remarkable is that the change happens over a very small range of induced strain yielding the anomalously large Grüneisen parameter, $\gamma_s(\varepsilon_c)$ (see Figure 2, lower panel).

More specifically, when sufficient strain was achieved, we observed a non-linear upturn in T_c and the Grüneisen parameter. Note, below 0.02 % some detwinning is still in process, which results in the critical temperature being quite slow to respond to strain at these smaller values. Such divergence could happen if a system is pushed towards a (quantum) phase transition as one expects in $SrTiO_3$ [64–67]. Comparing this experimental finding (Figure 2) with the theory (Figure 1) shows remarkably similar large divergent values and supports the microscopic ferroelectric soft-mode as the underlying superconducting mechanism in $SrTiO_3$.

In principle, there should be a scaling relation between responses of samples with different doping levels. However, the current experimental data does not allow for illustrating or ruling out the scaling relations. Smaller dimension and more precise sample preparation need to be developed; this is beyond the current work that focuses on orders-of-magnitude observations of the Grüneisen parameter.

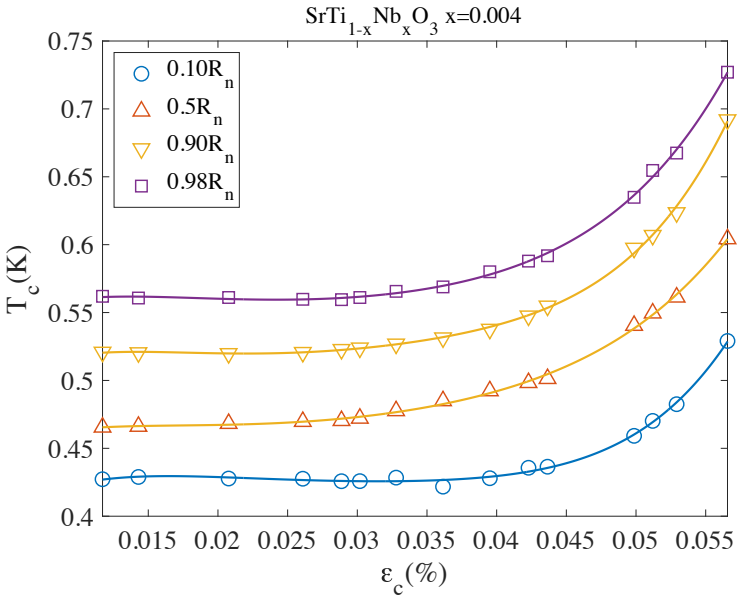

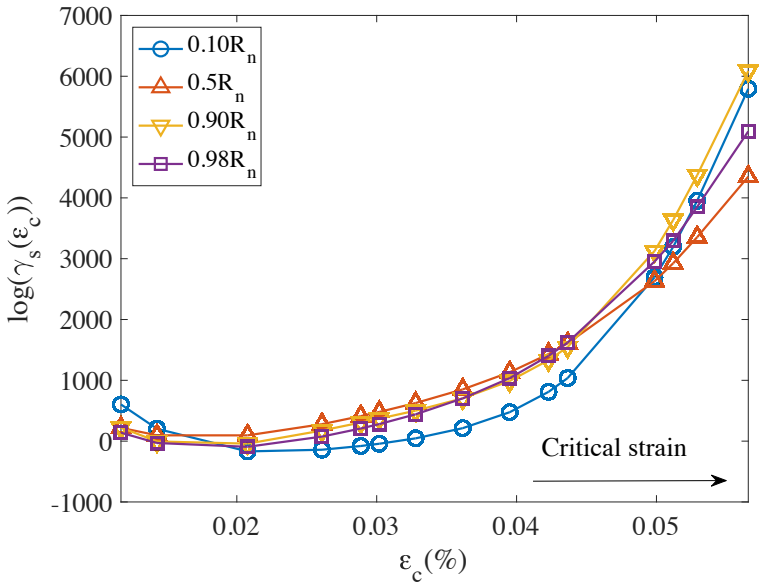

Figure 2. Experimental anomalous Grüneisen parameter, $\gamma_s(\varepsilon_c)$, determined from the derivative of experimentally measured superconducting T_c for Nb doped $SrTiO_3$. The crystals were strained in the c-axis direction using uniaxial tension. The derivative is based on 6-th degree polynomial smoothing fits (solid lines in the top panel). The Grüneisen parameter (bottom panel) shows anomalous growth reaching several thousand at maximal attained strains, which is higher than in many conventional and unconventional superconductors (lines are numerical derivatives of the fits to the experimental data in the upper panel, symbols are a guide for the eye to show at which strains T_c was actually measured). Note, the strain is in % (see also Appendix for raw data).

This is a striking finding. In conventional superconductors and even unconventional superconductors [31,34], the Grüneisen parameter estimated based on T_c is typically a few tens (unitless) [29–32,34]. It can be larger, many hundreds, only when another phase transition occurs, like topologically non-trivial changes in the electronic bands [33]. Divergent power-law behavior, $\propto (\varepsilon - \varepsilon_0)^{-1/2}$, is found in our *ab-initio* calculations. The value of the exponents is expected to be on the order of ½ in the soft-mode pairing model too (see Appendix and refs. [10,68]). Experimentally, we find that the observed superconducting Grüneisen parameter in strontium titanate follows $\propto \varepsilon^{\eta}$ with the exponent η on the order of 3-7. This is consistent with critical softening of the ferroelectric transverse phonon mode if a distribution of strains is taken into consideration in those models, see Appendix. However, the critical exponent is washed out in these bulk-averaged measurements of the resistive transition. Nevertheless our results are difficult to explain without the divergence.

In summary, this work shows that $\frac{d \ln T_c}{d \varepsilon_c}$ grows by orders of magnitude near the ferroelectric transition. This happens at the point at which the soft-mode frequency ω_0 vanishes,

suggesting a connection between these two macroscopic and microscopic parameters. In other words, the relationship between the anomalous responses of critical temperature and mode Grüneisen parameter to strain indicates that the ferroelectric soft-mode must be the key element in a theory that can correctly describe the pairing. This is true whether that theory is a direct [10,68], multi-phonon [21], screening [20] or any other scenario, even if they include couplings to other phonon modes.

The methods presented here can be applied to numerous other quantum materials such as high temperature and unconventional superconductors [69–72], quantum magnets [73–75], and topological matter [76–78]. Future experiments with induced strains in quantum materials may prove interesting, for example to directly test the mode Grüneisen parameters in scattering experiments [37,38,79] and determining a mesoscale and nanoscale response by microscopies such as a scanning SQUID [80]. These should reveal the true critical exponents, which are out-of-reach in the present bulk experiments, via micron or submicron characterization of the distribution of the superconducting properties. Beyond STO, this work can serve as a guide for broader future experiments on models of superconductivity in other doped ferroelectrics and superconducting polar metals.

Acknowledgements

We thank J. N. Hancock and V. Juričić for valuable suggestions. IS acknowledges the US State of Connecticut and the US DOD for partial support. UA was supported by the Swiss National Science Foundation Professorship Grants PP00P2_157615 and PP00P2_187185. Calculations were performed on UBELIX (http://www.id.unibe.ch/hpc), the HPC cluster at the University of Bern and at the Swiss Supercomputing Center (CSCS) under project s955. AB was supported by VILLUM FONDEN via the Centre of Excellence for Dirac Materials (Grant No. 11744), the European Research Council under the European Union's Seventh Framework Program Synergy HERO, and the Knut and Alice Wallenberg Foundation KAW 2018.0104.

Appendices

Appendix A. Additional details and comparison of phonon calculations to previous results

All calculations were performed for the tetragonal structure of $SrTiO_3$ with $a^0b^0c^-$ octahedral rotations. This distortion leads to a splitting of the three ferroelectric (FE) modes that would be triply degenerate in the cubic structure into a doubly degenerate set of in-plane FE modes and a non-degenerate FE mode along the strain axis (*c*-axis) that we focus on in this work. The PBEsol density functional adopted in our work for its good reproduction of lattice parameters still predicts a FE instability at relaxed lattice parameters and internal geometry. It is established

that this instability is suppressed either by finite temperature [82] or even by quantum fluctuations at 0K [59]. The instability can, however, also be tuned by strain. Tensile strain strengthens it, while under compression the ferroelectric instability is suppressed. Regarding the procedure, this is different from experiment, where we start from stable modes in the as-cooled material and approach the critical state by stretching the sample. Thus, the starting phase in experiment and the calculations are different and in terms of the protocol of the 'theoretical experiment' and the laboratory experiment, they proceed to deform the lattice from the opposite points on the strain axis. Physically, however, it is the same transition that is being examined and the phonons will have the same divergence of the mode Grüneisen parameter. In other words, the equilibrium phase in calculations is the ferroelectric phase, while in the experiment the equilibrium phase is the quantum paraelectric phase (suppressed ferroelectric phase), and the equilibrium theoretical and experimental lattice constant are different. In addition, our quasi-harmonic test calculations (data not shown) in the cubic phase showed an agreement with the experimental data (e.g. [81]) very similar to the one reported in ref. [82,83], supporting the accuracy of our results. On the calculation and experimental side, it would be interesting in future work to look at the thermal expansion and GP in a broader temperature-doping range, as in some works [40], but also in a detwinned state and more strain directions.

Appendix B. Sample resistance *vs.* strain

The original resistance data used to plot the critical temperature curves in Figure 2 and subsequently to derive the Grüneisen parameter is displayed in Figure 3. The main errors in determining the critical temperature come from irregularities in the *R(T)* curves associated with the sample inhomogeneities and domains pinned near contacts and edges. The irregularities result in variations on the order of ~5 mK. Regarding the noise level, we could determine T_c with about a single millikelvin precision.

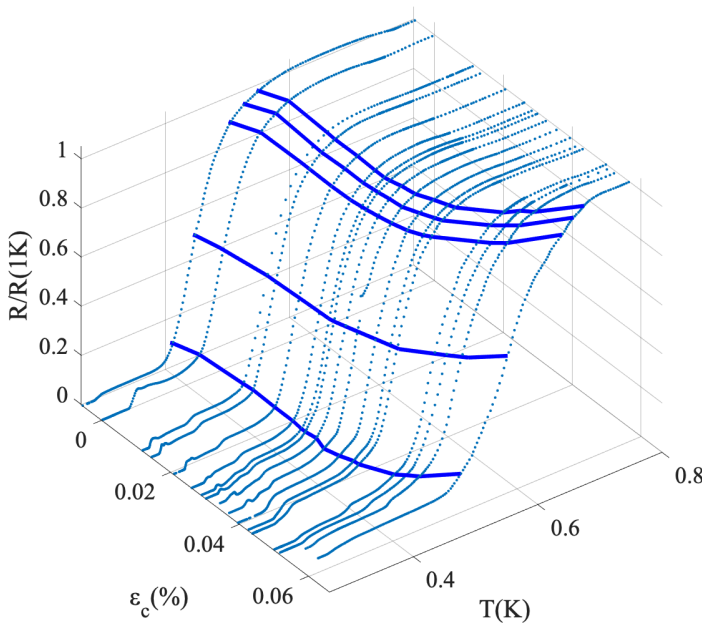

Figure 3. The normalized resistance data $R_n(T,\varepsilon) = R(T)/R_n$, where $R_n = R(T = 1\ K)$ from which the critical temperature shown in Figure 2 was derived. The blue solid contours represent definitions of T_c as $R_n(T,\varepsilon) = 0.1R_n, 0.5R_n, 0.9R_n, 0.95R_n$ and $0.98R_n$. The projection of these lines on $\varepsilon - T$ plane is plotted in Figure 2

Appendix C. *log-log* plot of the Grüneisen parameter

As explained in the main text, the experimental Grüneisen parameter deviates from the theorical one likely due to the distribution of strains, see Figure 4.

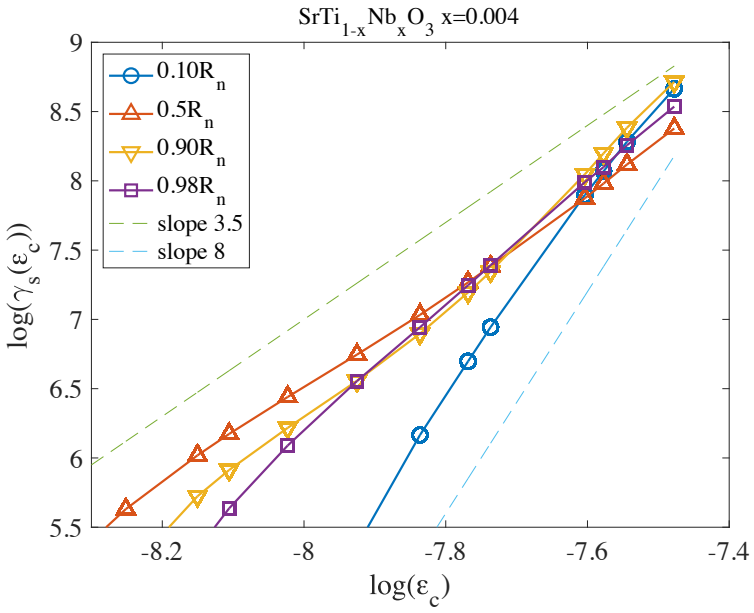

Figure 4. The logarithmic scale plot of the Grüneisen parameter from Figure 2. The $\gamma_s \propto \varepsilon^{\eta}$ functional form rather than $\propto (\varepsilon - \varepsilon_0)^{-\eta}$ is apparent. The values of the phenomenological η for demonstration purpose are compared to a slope of 3.5 and 8 shown by the dashed lines.

Appendix D. Derivation of the Grüneisen parameter and the effect of distribution of strains

We introduce the Grüneisen-like parameter that measures the dependence of the condensate energy $F_c = F_s - F_n$ where F_s, F_n are the respective free energies of superconducting state and normal state. Within a BCS-like approach, $F_c = N_0\Delta_0^2/2$, where N_0 is the density of states near Fermi level, and Δ_0 is the superconducting order parameter. Furthermore, $\Delta_0 = O(1)\cdot T_c$. We next take the logarithmic derivative of the condensate energy with respect to volume: $\frac{d\ln(F_c)}{d\ln V} = \frac{d(\ln(N_0)+2\ln(\Delta_0))}{d\ln(V)}$. Typically, for strains reported in the experimental part on the order of 10^{-4}, the first term $d\ln(N_0)/d\ln(V)$ is expected to be small. The second term is then defined as the thermodynamic Grüneisen parameter:

$$\frac{2d\ln(\Delta_0)}{d\ln V} \approx \frac{2d\ln(T_c)}{d\ln V} \equiv \gamma_s(V).$$

To match to the experimental conditions, rather than working with volume derivatives, we define an analogous thermodynamic Grüneisen parameter for strain:

$$\frac{2d\ln(T_c)}{d\ln\varepsilon} \equiv \gamma_s(\varepsilon).$$

Next, let us show how this thermodynamic parameter can be expressed in the soft-mode quantum critical superconducting pairing ansatz introduced by Edge et al. [10]. The critical

temperature of strontium titanate in this model depends on the soft-phonon frequency, ω_0, and density of states $\alpha^2F(\omega_0)$, as $T_c = \epsilon_F e^{-\frac{\omega_0}{\alpha^2F(\omega_0)}}$. Taking the logarithmic derivative of this T_c yields

$$\gamma_s(\varepsilon) = \frac{2d\ln(\mathrm{T}_c)}{d\ln\varepsilon} = -\frac{2d(\frac{\omega_0}{\alpha^2F(\omega_0)})}{d\ln\varepsilon} + \frac{2d\epsilon_F}{d\ln\varepsilon}.$$

The second term is assumed to be small. In addition, $\alpha^2F(\omega_0)$ is assumed to be independent of ω_0. Using $\omega_0 = \bar{\omega}|\varepsilon_0 - \varepsilon|^{z\nu}$ for the quantum critical scenario in the first term we obtain that the Grüneisen parameter γ_s can be expressed as

$$\gamma_s = \frac{2d\ln T_c}{d\ln\varepsilon} \approx -2\frac{\bar{\omega}z\nu}{\alpha^2F(\omega_0)}|\varepsilon - \varepsilon_0|^{z\nu-1} \sim O(1)\cdot|\varepsilon - \varepsilon_0|^{\alpha}\,.$$

In previous models of BCS like pairing we held $\alpha = -1$. However, here this assumption is not needed, thus we can proceed with the general ansatz that $\gamma_s \sim |\varepsilon - \varepsilon_0|^{\alpha}$.

Next we assume that there is an effective distribution of critical values of strain ε_0, which occurs, for instance, due to tetragonal domains experiencing different local strain and is given by

$$P(\varepsilon_0) = \Theta(a - \varepsilon_0)\varepsilon_0^{\mu}$$

Here, the step function is introduced to account for the cut off of the critical values at some value a that is assumed to be a maximum local value assuming optimal conditions for the uniformity of the strain (i.e. full sample detwinning and geometrically uniform strain, which are actually quite hard to achieve experimentally). Hence the assumption is that the critical regions in the sample will start appearing at lower average strain than the true critical strain.

In general, the $P(\varepsilon_0)$ distribution is not known experimentally, and we assume for simplicity it is given by the power law to demonstrate the point that the critical exponent will be hindered by the distributions of strains. The average Grüneisen-like parameter would take into account the distribution of critical strains. The total averaged $<\gamma_s(\varepsilon)>$ would thus be

$$<\gamma_s(\varepsilon)> \sim \int_0^a d\varepsilon_0\, \varepsilon_0^{\mu}\,|\varepsilon - \varepsilon_0|^{\alpha}$$

After rearranging and simplifying using saddle point approximation, we obtain the effective strain

$$\varepsilon_0^* = \frac{\mu\,\varepsilon}{\mu+\alpha}.$$

Using the effective strain, we find the averaged Grüneisen-like parameter

$$<\gamma_s(\varepsilon)> \sim \varepsilon^{\mu+\alpha+1}$$

For mean-field-like result as in BCS theory we would expect to have $\alpha = -1$. Hence we would expect a linear log-log fit of averaged Grüneisen-like parameter for $\log(<\gamma_s(\varepsilon)>)$ *vs.* $\log\,\varepsilon$, as is indeed the case in Figure 4. From this figure we infer that $\mu + \alpha + 1 \cong 3.5$ to 8. A more precise microscopic modeling of the strain dependence of $<\gamma_s(\varepsilon)>$ would require a detailed

knowledge of strain distribution and inhomogeneities in the sample. Preliminarily, we do observe inhomogeneities in the superconducting state with a scanning SQUID that will be presented in a separate future publication.

References

[1] P. Lu, J.-S. Kim, J. Yang, H. Gao, J. Wu, D. Shao, B. Li, D. Zhou, J. Sun, D. Akinwande, D. Xing, and J.-F. Lin, *Origin of Superconductivity in the Weyl Semimetal WT_2 under Pressure*, Phys. Rev. B **94**, 224512 (2016).

[2] P. Sharma, F.-X. Xiang, D.-F. Shao, D. Zhang, E. Y. Tsymbal, A. R. Hamilton, and J. Seidel, *A Room-Temperature Ferroelectric Semimetal*, Sci. Adv. **5**, eaax5080 (2019).

[3] K. Ueno, S. Nakamura, H. Shimotani, G. Yuan, N. Kimura, T. Nojima, H. Aoki, Y. Iwasa, and M. Kawasaki, *Discovery of Superconductivity in $KTaO_3$ by Electrostatic Carrier Doping*, Nat. Nanotechnol. **6**, 408 (2011).

[4] E. Bustarret, *Superconductivity in Doped Semiconductors*, Supercond. Mater. Conv. Unconv. Undetermined **514**, 36 (2015).

[5] M. L. Jin, F. Sun, L. Y. Xing, S. J. Zhang, S. M. Feng, P. P. Kong, W. M. Li, X. C. Wang, J. L. Zhu, Y. W. Long, H. Y. Bai, C. Z. Gu, R. C. Yu, W. G. Yang, G. Y. Shen, Y. S. Zhao, H. K. Mao, and C. Q. Jin, *Superconductivity Bordering Rashba Type Topological Transition*, Sci. Rep. **7**, 39699 (2017).

[6] J. I. Facio, D. Efremov, K. Koepernik, J.-S. You, I. Sodemann, and J. van den Brink, *Strongly Enhanced Berry Dipole at Topological Phase Transitions in BiTeI*, Phys. Rev. Lett. **121**, 246403 (2018).

[7] M. N. Gastiasoro, J. Ruhman, and R. M. Fernandes, *Superconductivity in Dilute $SrTiO_3$: A Review*, Ann. Phys. 168107 (2020).

[8] P. Chandra, G. G. Lonzarich, S. E. Rowley, and J. F. Scott, *Prospects and Applications near Ferroelectric Quantum Phase Transitions: A Key Issues Review*, Rep Prog Phys **80**, 112502 (2017).

[9] Y. Cao, V. Fatemi, S. Fang, K. Watanabe, T. Taniguchi, E. Kaxiras, and P. Jarillo-Herrero, *Unconventional Superconductivity in Magic-Angle Graphene Superlattices*, Nature **556**, 43 (2018).

[10] J. M. Edge, Y. Kedem, U. Aschauer, N. A. Spaldin, and A. V. Balatsky, *Quantum Critical Origin of the Superconducting Dome in $SrTiO_3$*, Phys. Rev. Lett. **115**, 247002 (2015).

[11] J. Ruhman and P. A. Lee, *Superconductivity at Very Low Density: The Case of Strontium Titanate*, Phys Rev B **94**, 224515 (2016).

[12] L. P. Gor'kov, *Phonon Mechanism in the Most Dilute Superconductor N-Type $SrTiO_3$*, Proc Natl Acad Sci USA **113**, 4646 (2016).

[13] L. P. Gor'kov, *Back to Mechanisms of Superconductivity in Low-Doped Strontium Titanate*, J Supercond Nov Mag **30**, 845 (2017).

[14] P. Wölfle and A. V. Balatsky, *Superconductivity at Low Density near a Ferroelectric Quantum Critical Point: Doped $SrTiO_3$*, Phys. Rev. B **98**, 104505 (2018).

[15] J. R. Arce-Gamboa and G. G. Guzmán-Verri, *Quantum Ferroelectric Instabilities in Superconducting $SrTiO_3$*, Phys. Rev. Mater. **2**, 104804 (2018).

[16] S. Kanasugi and Y. Yanase, *Spin-Orbit-Coupled Ferroelectric Superconductivity*, Phys. Rev. B **98**, 024521 (2018).

[17] Y. Kedem, *Novel Pairing Mechanism for Superconductivity at a Vanishing Level of Doping Driven by Critical Ferroelectric Modes*, Phys. Rev. B **98**, 220505 (2018).
[18] S. Kanasugi and Y. Yanase, *Multiorbital Ferroelectric Superconductivity in Doped $SrTiO_3$*, Phys. Rev. B **100**, 094504 (2019).
[19] M. N. Gastiasoro, A. V. Chubukov, and R. M. Fernandes, *Phonon Mediated Superconductivity in Low Carrier-Density Systems*, Phys Rev B **99**, 094524 (2019).
[20] S. N. Klimin, J. Tempere, J. T. Devreese, J. He, C. Franchini, and G. Kresse, *Superconductivity in SrTiO3: Dielectric Function Method for Non-Parabolic Bands*, J. Supercond. Nov. Magn. **32**, 2739 (2019).
[21] D. van der Marel, F. Barantani, and C. W. Rischau, *Possible Mechanism for Superconductivity in Doped $SrTiO_3$*, Phys. Rev. Res. **1**, 013003 (2019).
[22] A. Stucky, G. W. Scheerer, Z. Ren, D. Jaccard, J.-M. Poumirol, C. Barreteau, E. Giannini, and D. van der Marel, *Isotope Effect in Superconducting N-Doped $SrTiO_3$*, Sci Rep **6**, 37582 (2016).
[23] C. W. Rischau, X. Lin, C. P. Grams, D. Finck, S. Harms, J. Engelmayer, T. Lorenz, Y. Gallais, B. Fauqué, J. Hemberger, and K. Behnia, *A Ferroelectric Quantum Phase Transition inside the Superconducting Dome of $Sr_{1-x}Ca_xTiO_{3-\delta}$*, Nat. Phys. **13**, 643 (2017).
[24] Y. Tomioka, N. Shirakawa, K. Shibuya, and I. H. Inoue, *Enhanced Superconductivity Close to a Non-Magnetic Quantum Critical Point in Electron-Doped Strontium Titanate*, Nat. Comm **10**, 738 (2019).
[25] K. Ahadi, L. Galletti, Y. Li, S. Salmani-Rezaie, W. Wu, and S. Stemmer, *Enhancing Superconductivity in $SrTiO_3$ Films with Strain*, Sci. Adv. **5**, eaaw0120 (2019).
[26] C. Herrera, J. Cerbin, A. Jayakody, K. Dunnett, A. V. Balatsky, and I. Sochnikov, *Strain-Engineered Interaction of Quantum Polar and Superconducting Phases*, Phys. Rev. Mater. **3**, 124801 (2019).
[27] C. Herrera and I. Sochnikov, *A Local Maximum in the Superconducting Transition Temperature of Nb-Doped Strontium Titanate Under Uniaxial Compressive Stress*, J. Supercond. Nov. Magn. **33**, 191 (2020).
[28] C. Enderlein, J. F. de Oliveira, D. A. Tompsett, E. B. Saitovitch, S. S. Saxena, G. G. Lonzarich, and S. E. Rowley, *Superconductivity Mediated by Polar Modes in Ferroelectric Metals*, Nat. Commun. **11**, 4852 (2020).
[29] C. L. Watlington, J. W. Cook, and M. J. Skove, *Effect of Large Uniaxial Stress on the Superconducting Transition Temperature of Zinc and Cadmium*, Phys. Rev. B **15**, 1370 (1977).
[30] V. I. Dotsenko, I. F. Kislyak, V. T. Petrenko, M. A. Tikhonovsky, A. M. Shkilko, L. N. Zagoruiko, and L. M. Rogozyanskaya, *Static Stress Effects in Superconducting Composites: Part II. Effect of Uniaxial Tensile and Compressive Stresses on Critical Temperatures of Cu–Nb, Cu–NbTi, and Bronze–Nb_3Sn Composites*, Cryogenics **41**, 225 (2001).
[31] O. M. Dix, A. G. Swartz, R. J. Zieve, J. Cooley, T. R. Sayles, and M. B. Maple, *Anisotropic Dependence of Superconductivity on Uniaxial Pressure in $CeIrIn_5$*, Phys Rev Lett **102**, 197001 (2009).
[32] K. Kikuchi, T. Isono, M. Kojima, H. Yoshimoto, T. Kodama, W. Fujita, K. Yokogawa, H. Yoshino, K. Murata, T. Kaihatsu, H. Akutsu, and J. Yamada, *Uniaxial Strain Orientation*

Dependence of Superconducting Transition Temperature (T_c) and Critical Superconducting Pressure (P_c) in β-(BDA-TTP)$_2$I$_3$, J. Am. Chem. Soc. **133**, 19590 (2011).
[33] A. Steppke, L. Zhao, M. E. Barber, T. Scaffidi, F. Jerzembeck, H. Rosner, A. S. Gibbs, Y. Maeno, S. H. Simon, A. P. Mackenzie, and C. W. Hicks, *Strong Peak in T_c of Sr_2RuO_4 under Uniaxial Pressure*, Science **355**, (2017).
[34] M. Mito, K. Ogata, H. Goto, K. Tsuruta, K. Nakamura, H. Deguchi, T. Horide, K. Matsumoto, T. Tajiri, H. Hara, T. Ozaki, H. Takeya, and Y. Takano, *Uniaxial Strain Effects on the Superconducting Transition in Re-Doped Hg-1223 Cuprate Superconductors*, Phys. Rev. B **95**, 064503 (2017).
[35] P. Malinowski, Q. Jiang, J. J. Sanchez, J. Mutch, Z. Liu, P. Went, J. Liu, P. J. Ryan, J.-W. Kim, and J.-H. Chu, *Suppression of Superconductivity by Anisotropic Strain near a Nematic Quantum Critical Point*, Nat. Phys. (2020).
[36] R. Küchler, N. Oeschler, P. Gegenwart, T. Cichorek, K. Neumaier, O. Tegus, C. Geibel, J. A. Mydosh, F. Steglich, L. Zhu, and Q. Si, *Divergence of the Gr\"uneisen Ratio at Quantum Critical Points in Heavy Fermion Metals*, Phys. Rev. Lett. **91**, 066405 (2003).
[37] J. N. Hancock, C. Turpen, Z. Schlesinger, G. R. Kowach, and A. P. Ramirez, *Unusual Low-Energy Phonon Dynamics in the Negative Thermal Expansion Compound ZrW_2O_8*, Phys. Rev. Lett. **93**, 225501 (2004).
[38] S. U. Handunkanda, E. B. Curry, V. Voronov, A. H. Said, G. G. Guzmán-Verri, R. T. Brierley, P. B. Littlewood, and J. N. Hancock, *Large Isotropic Negative Thermal Expansion above a Structural Quantum Phase Transition*, Phys. Rev. B **92**, 134101 (2015).
[39] R. Bhandia, T. Siegrist, T. Besara, and G. M. Schmiedeshoff, *Grüneisen Divergence near the Structural Quantum Phase Transition in ScF_3*, Philos. Mag. **99**, 631 (2019).
[40] J. Engelmayer, X. Lin, F. Koç, C. P. Grams, J. Hemberger, K. Behnia, and T. Lorenz, *Ferroelectric Order versus Metallicity in $Sr_{1-x}Ca_xTiO_{3-\delta}$ (X=0.009)*, Phys. Rev. B **100**, 195121 (2019).
[41] R. W. Munn, *Grüneisen Functions for Some Type-I Superconductors*, Phys. Rev. **178**, 677 (1969).
[42] R. Mittal, M. K. Gupta, and S. L. Chaplot, *Phonons and Anomalous Thermal Expansion Behaviour in Crystalline Solids*, Prog. Mater. Sci. **92**, 360 (2018).
[43] L. Zhu, M. Garst, A. Rosch, and Q. Si, *Universally Diverging Grüneisen Parameter and the Magnetocaloric Effect Close to Quantum Critical Points*, Phys RevLett **91**, 066404 (2003).
[44] T. H. K. Barron and R. W. Munn, *Analysis of the Thermal Expansion of Anisotropic Solids: Application to Zinc*, Philos. Mag. J. Theor. Exp. Appl. Phys. **15**, 85 (1967).
[45] C. Herrera and I. Sochnikov, *Precision Measurements of the AC Field Dependence of the Superconducting Transition in Strontium Titanate*, J. Supercond. Nov. Magn. **33**, 201 (2020).
[46] C. P. Romao, *Anisotropic Thermal Expansion in Flexible Materials*, Phys. Rev. B **96**, 134113 (2017).
[47] J. F. Scott and H. Ledbetter, *Interpretation of Elastic Anomalies in $SrTiO_3$ at 37K*, Z. Für Phys. B Condens. Matter **104**, 635 (1997).
[48] J. L. M. van Mechelen, D. van der Marel, C. Grimaldi, A. B. Kuzmenko, N. P. Armitage, N. Reyren, H. Hagemann, and I. I. Mazin, *Electron-Phonon Interaction and Charge Carrier Mass Enhancement in $SrTiO_3$*, Phys. Rev. Lett. **100**, 226403 (2008).

[49] C. Cancellieri, A. S. Mishchenko, U. Aschauer, A. Filippetti, C. Faber, O. S. Barišić, V. A. Rogalev, T. Schmitt, N. Nagaosa, and V. N. Strocov, *Polaronic Metal State at the $LaAlO_3/SrTiO_3$ Interface*, Nat. Commun. **7**, 10386 (2016).
[50] G. Kresse and J. Hafner, *Ab Initio Molecular Dynamics for Liquid Metals*, Phys. Rev. B **47**, 558 (1993).
[51] G. Kresse and J. Hafner, *Ab Initio Molecular-Dynamics Simulation of the Liquid-Metal--Amorphous-Semiconductor Transition in Germanium*, Phys. Rev. B **49**, 14251 (1994).
[52] G. Kresse and J. Furthmüller, *Efficiency of Ab-Initio Total Energy Calculations for Metals and Semiconductors Using a Plane-Wave Basis Set*, Comput. Mater. Sci. **6**, 15 (1996).
[53] G. Kresse and J. Furthmüller, *Efficient Iterative Schemes for Ab Initio Total-Energy Calculations Using a Plane-Wave Basis Set*, Phys. Rev. B **54**, 11169 (1996).
[54] J. P. Perdew, A. Ruzsinszky, G. I. Csonka, O. A. Vydrov, G. E. Scuseria, L. A. Constantin, X. Zhou, and K. Burke, *Restoring the Density-Gradient Expansion for Exchange in Solids and Surfaces*, Phys. Rev. Lett. **100**, 136406 (2008).
[55] P. E. Blöchl, *Projector Augmented-Wave Method*, Phys. Rev. B **50**, 17953 (1994).
[56] G. Kresse and D. Joubert, *From Ultrasoft Pseudopotentials to the Projector Augmented-Wave Method*, Phys. Rev. B **59**, 1758 (1999).
[57] A. M. Glazer, *The Classification of Tilted Octahedra in Perovskites*, Acta Crystallogr. Sect. B **28**, 3384 (1972).
[58] H. J. Monkhorst and J. D. Pack, *Special Points for Brillouin-Zone Integrations*, Phys. Rev. B **13**, 5188 (1976).
[59] W. Zhong and D. Vanderbilt, *Effect of Quantum Fluctuations on Structural Phase Transitions in $SrTiO_3$ and $BaTiO_3$*, Phys. Rev. B **53**, 5047 (1996).
[60] D. Vanderbilt and W. Zhong, *First-Principles Theory of Structural Phase Transitions for Perovskites: Competing Instabilities*, Ferroelectrics **206**, 181 (1998).
[61] F. Hardy, C. Meingast, V. Taufour, J. Flouquet, H. v. Löhneysen, R. A. Fisher, N. E. Phillips, A. Huxley, and J. C. Lashley, *Two Magnetic Grüneisen Parameters in the Ferromagnetic Superconductor UGe_2*, Phys Rev B **80**, 174521 (2009).
[62] C. Fujii, S. Simayi, K. Sakano, C. Sasaki, M. Nakamura, Y. Nakanishi, K. Kihou, M. Nakajima, C.-H. Lee, A. Iyo, H. Eisaki, S. Uchida, and M. Yoshizawa, *Anisotropic Grüneisen Parameter and Diverse Order Parameter Fluctuations in Iron-Based Superconductor $Ba(Fe_{1-x}Co_x)_2As_2$*, J. Phys. Soc. Jpn. **87**, 074710 (2018).
[63] D. Davino, J. Franklin, and I. Sochnikov, *Millikelvin-Compatible Apparatus for Studies of Quantum Materials under Uniaxial Stress*, AIP Adv. **9**, 125244 (2019).
[64] H. Uwe and T. Sakudo, *Stress-Induced Ferroelectricity and Soft Phonon Modes in $SrTiO_3$*, Phys Rev B **13**, 271 (1976).
[65] K. A. Müller and H. Burkard, *$SrTiO_3$: An Intrinsic Quantum Paraelectric below 4 K*, Phys. Rev. B **19**, 3593 (1979).
[66] F. He, B. O. Wells, and S. M. Shapiro, *Strain Phase Diagram and Domain Orientation in $SrTiO_3$ Thin Films*, Phys Rev Lett **94**, 176101 (2005).
[67] Y. L. Li, S. Choudhury, J. H. Haeni, M. D. Biegalski, A. Vasudevarao, A. Sharan, H. Z. Ma, J. Levy, V. Gopalan, S. Trolier-McKinstry, D. G. Schlom, Q. X. Jia, and L. Q. Chen, *Phase Transitions and Domain Structures in Strained Pseudocubic (100) $SrTiO_3$ Thin Films*, Phys. Rev. B **73**, 184112 (2006).

[68] K. Dunnett, A. Narayan, N. A. Spaldin, and A. V. Balatsky, *Strain and Ferroelectric Soft-Mode Induced Superconductivity in Strontium Titanate*, Phys. Rev. B **97**, 144506 (2018).
[69] I. Sochnikov, A. Shaulov, Y. Yeshurun, G. Logvenov, and I. Bozovic, *Large Oscillations of the Magnetoresistance in Nanopatterned High-Temperature Superconducting Films*, Nat. Nano **5**, 516 (2010).
[70] J.-H. Chu, H.-H. Kuo, J. G. Analytis, and I. R. Fisher, *Divergent Nematic Susceptibility in an Iron Arsenide Superconductor*, Science **337**, 710 (2012).
[71] P. Zhou, L. Chen, Y. Liu, I. Sochnikov, A. T. Bollinger, M.-G. Han, Y. Zhu, X. He, I. Božović, and D. Natelson, *Electron Pairing in the Pseudogap State Revealed by Shot Noise in Copper Oxide Junctions*, Nature **572**, 493 (2019).
[72] M. D. Bachmann, G. M. Ferguson, F. Theuss, T. Meng, C. Putzke, T. Helm, K. R. Shirer, Y.-S. Li, K. A. Modic, M. Nicklas, M. König, D. Low, S. Ghosh, A. P. Mackenzie, F. Arnold, E. Hassinger, R. D. McDonald, L. E. Winter, E. D. Bauer, F. Ronning, B. J. Ramshaw, K. C. Nowack, and P. J. W. Moll, *Spatial Control of Heavy-Fermion Superconductivity in $CeIrIn_5$*, Science **366**, 221 (2019).
[73] S. Manna, A. Kamlapure, L. Cornils, T. Hänke, E. M. J. Hedegaard, M. Bremholm, B. B. Iversen, P. Hofmann, J. Wiebe, and R. Wiesendanger, *Evidence for Interfacial Superconductivity in a Bi-Collinear Antiferromagnetically Ordered FeTe Monolayer on a Topological Insulator*, ArXiv160603249 Cond-Mat (2016).
[74] M. Ruminy, M. N. Valdez, B. Wehinger, A. Bosak, D. T. Adroja, U. Stuhr, K. Iida, K. Kamazawa, E. Pomjakushina, D. Prabakharan, M. K. Haas, L. Bovo, D. Sheptyakov, A. Cervellino, R. J. Cava, M. Kenzelmann, N. A. Spaldin, and T. Fennell, *First-Principles Calculation and Experimental Investigation of Lattice Dynamics in the Rare-Earth Pyrochlores $R_2Ti_2O_7$ (R = Tb, Dy, Ho)*, Phys. Rev. B **93**, 214308 (2016).
[75] F. Bahrami, W. Lafargue-Dit-Hauret, O. I. Lebedev, R. Movshovich, H.-Y. Yang, D. Broido, X. Rocquefelte, and F. Tafti, *Thermodynamic Evidence of Proximity to a Kitaev Spin Liquid in $Ag_3LiIr_2O_6$*, Phys. Rev. Lett. **123**, 237203 (2019).
[76] I. Sochnikov, A. J. Bestwick, J. R. Williams, T. M. Lippman, I. R. Fisher, D. Goldhaber-Gordon, J. R. Kirtley, and K. A. Moler, *Direct Measurement of Current-Phase Relations in Superconductor/Topological Insulator/Superconductor Junctions*, Nano Lett. **13**, 3086 (2013).
[77] I. Sochnikov, L. Maier, C. A. Watson, J. R. Kirtley, C. Gould, G. Tkachov, E. M. Hankiewicz, C. Brüne, H. Buhmann, L. W. Molenkamp, and K. A. Moler, *Nonsinusoidal Current-Phase Relationship in Josephson Junctions from the 3D Topological Insulator HgTe*, Phys. Rev. Lett. **114**, 066801 (2015).
[78] B. Roy, R.-J. Slager, and V. Juričić, *Global Phase Diagram of a Dirty Weyl Liquid and Emergent Superuniversality*, Phys. Rev. X **8**, 031076 (2018).
[79] R. Mittal, S. L. Chaplot, H. Schober, and T. A. Mary, *Origin of Negative Thermal Expansion in Cubic ZrW_2O_8 Revealed by High Pressure Inelastic Neutron Scattering*, Phys. Rev. Lett. **86**, 4692 (2001).
[80] D. V. Christensen, Y. Frenkel, Y. Z. Chen, Y. W. Xie, Z. Y. Chen, Y. Hikita, A. Smith, L. Klein, H. Y. Hwang, N. Pryds, and B. Kalisky, *Strain-Tunable Magnetism at Oxide Domain Walls*, Nat. Phys. (2018).

[81] W. G. Stirling, *Neutron Inelastic Scattering Study of the Lattice Dynamics of Strontium Titanate: Harmonic Models*, J Phys C Sol State Phys **5**, 2711 (1972).
[82] T. Tadano and S. Tsuneyuki, *Self-Consistent Phonon Calculations of Lattice Dynamical Properties in Cubic $SrTiO_3$ with First-Principles Anharmonic Force Constants*, Phys. Rev. B **92**, 054301 (2015).
[83] L. Feng, T. Shiga, and J. Shiomi, *Phonon Transport in Perovskite $SrTiO_3$ from First Principles*, Appl. Phys. Express **8**, 071501 (2015).